Advanced Passive Radiator for Spaceborne Cryogenic Cooling

Steven Bard*
Jet Propulsion Laboratory, California Institute of Technology, Pasadena, California

A novel design to improve the cooling capability of spaceborne cryogenic passive radiators is described herein. The design is based on the use of lightweight angled radiation shields, low-conductance structural supports, and a separate detachable launch support system to reduce the parasitic heat leaks from the warm spacecraft to the cold radiator. The effectiveness of this design is demonstrated by thermal vacuum chamber experiments which indicate that the angled radiation shield assembly has an effective emittance that is an order of magnitude lower than that of the best existing multilayer insulation used in flight. Performance predictions based on the experiments and analytical model indicate that an advanced passive radiator design based on the technology developments described here would be between 10 and 57% of the size and 10 and 36% of the mass of the best "state-of-the-art" passive radiators. Utilization of this technology in radiator designs would make lower temperatures (<60 K) and larger heat loads practical. The cooling requirements of many new spaceborne instruments could be accommodated by application of this new passive radiator design.

Nomenclature

A_r = surface area of radiator plate
C_{ij} = conductance from node i to node j
$\mathfrak{F}_{i-j}$ = radiation interchange factor from node to i to node j
P = power input to radiator plate (to simulate detector heat load)
T_i = temperature of node i
ϵ = emissivity
ϵ_{eff} = effective emissivity of radiation shields
σ = Stefan-Boltzmann constant = 5.67×10^{-8} W/m^2-K^4

Subscripts

E = environment
F = frame
R = radiator plate
S = planet shade

Introduction

IN recent years, there has been considerable growth in the use of spaceborne instruments that require cryogenic cooling to obtain adequate detector sensitivities.[1,2] In the past, passive radiators have provided the cooling for most of the applications requiring detector temperatures of 90 K and greater.[1-3] The wide use of radiative coolers has been due to their relative simplicity, low mass, negligible power consumption, and high reliability. Unfortunately, recent demands for lower sensor temperatures combined with the use of large detector arrays are exceeding the capabilities of conventional radiant coolers.

The many attractive features of passive radiators and the limited lifetimes of alternative cooling techniques (e.g., mechanical refrigerators and solid cryogens)[1] make it worthwhile to pursue improvements to radiative cooler designs. This paper describes the development and preliminary thermal engineering model testing of an advanced passive radiator that is smaller, lighter, can achieve lower temperatures, and reject greater heat loads than "state-of-the-art" radiators and can accommodate many of the new spaceborne instrument needs.

Submitted Sept. 17, 1982; revision received July 27, 1983.

*Member of Technical Staff, Applied Mechanics Technology Section. Member AIAA.

Concept

The major problem in achieving cryogenic temperatures with passive radiator systems is in thermally isolating the system from the spacecraft and external environment. To reduce external heating of a radiator, the cold stage must be shielded from the sun, Earth (or other planet), and other spacecraft surfaces.[1,3-8] To reduce internal heat leaks from the hot spacecraft to the cold radiator, conventional radiative coolers[1,3,4] are usually built with two or more stages that are thermally isolated from each other by multilayer insulation and low-conductive support posts. Each successive stage, consisting of a high-emittance plate or disk, is surrounded by a colder boundary temperature. The sensor to be cooled is attached to the coldest stage. This staging technique reduces parasitic heat leakage to the cold stage. However, an examination of the heat balances of past multistaged radiators[3,7] indicates that even with staging, the conductive and radiative parasitic heat leaks are usually the dominant cold stage heat loads.

The advanced passive radiator uses two separate techniques to reduce the parasitic conductive and radiative heat leaks to the cold radiator stage.[9] The conductive heat flows are reduced by designing a separate structural support system that can accommodate launch loads. In orbit, the launch support system detaches mechanically and thermally from the radiator plate. A low-conductance tension support system, which can sustain the flight structural loads, remains. The radiative heat leaks are reduced by a novel arrangement of lightweight, low-emittance, low-conductance, highly specular and reflective angled radiation shields. Adjacent shields are arranged with an included angle of about 1.5 deg, creating large V-groove cavities with the wider opening viewing space. Thermal radiation from the hot spacecraft side is intercepted and reflected by the shields and directed out the opening to the cold sink of space, as indicated in Fig. 1. The multiple reflections within a V-groove cavity act to augment the emissive power of the cavity relative to that of a plane surface stretched across its opening. The use of several lightweight shields creates a staging effect, but these stages are much less massive than the heavy metal plates used on conventional multistaged radiators, thereby greatly reducing the overall cooler size and mass.

Figure 2 shows a conceptual radiator plate surrounded by four angled shields. The shade shown in the figure is to prevent direct solar, albedo, planetary, or spacecraft emission onto the cold stage plate or into the V-groove cavities formed by the shields. The shields, constructed from lightweight

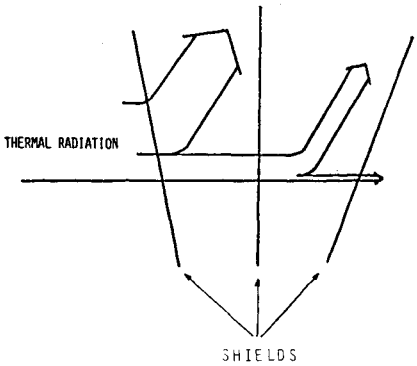

Fig. 1 Angled radiation shield concept.

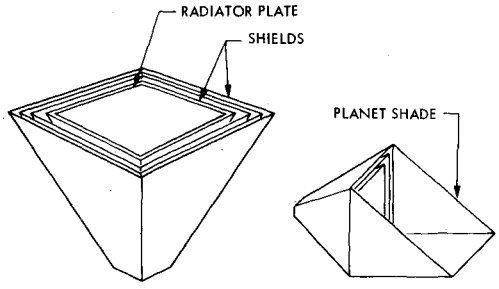

Fig. 2 Advanced passive radiator with angled radiation shields.

aluminized Mylar sheets, and the cold stage plate are supported by low-conductance tendons at each corner connected to an outer support structure.

A detailed design of a detachable launch support mechanism has not been performed to date, but several concepts have been generated. Several spacecraft in the past have successfully used detachable launch supports for some components. For example, the SEASAT synthetic aperture radar (SAR) antenna was caged by a launch support mechanism that was then automatically detached in orbit. In one scheme, the launch support mechanism for the advanced passive radiator may be made integral with a deployable planet shade that cages the radiator plate during launch and is designed to automatically detach and open to its shading orientation in orbit. No penetrations of the radiation shields by launch supports, which would degrade performance, are required by this design. Much effort is still required in order to develop all the fine points of the design, but a detachable launch support system is not considered a new technology item.

Initially, a 39-node, steady-state, analytical thermal model was developed to confirm the design.[2] Monte Carlo techniques[2] were used to model the specular shield surfaces. A laboratory test of a section of a radiator containing the new angled shield concept was conducted, and the results were reported previously.[2] The concept experiment and analytical model indicated the effectiveness of the radiation shielding technique and encouraged further development of the approach.

To further confirm the concept, the analytical model and the concept test results were used as a design tool to aid in fabrication of an advanced passive radiator thermal engineering model. The advanced passive radiator is adaptable to any orbit and environment where radiative coolers are practical. However, in order to make the comparison with other coolers more tangible, the thermal engineering model was designed for specific application to a flight experiment. The stringent requirements of the advanced moisture and temperature sounder (AMTS) cooler[8] were chosen as the design goal. The AMTS is an 833-km, near-polar, 8:30 a.m., sun-synchronous Earth-orbiting infrared spectrometer. The conceptual design of a state-of-the-art conventional radiator for AMTS can achieve a cold stage temperature of 63 K, with a detector heat load of 258 mW (Ref. 8). The radiator thermal engineering model described in the next section is approximately a 0.58 linear scale model of the advanced passive radiator, which can achieve the same performance as the AMTS conceptual cooler.

Experiment

Figure 3 shows a photo of the advanced passive radiator thermal engineering model. Figure 4 shows an exploded view of the radiator, which should aid in understanding its assembly. The $58.4 \times 30.5 \times 0.127$-cm cold stage radiator plate is coated with Chemglaze Z-306 high-emittance black paint ($\epsilon = 0.85$-0.9 at 77 K). The reverse side of the plate is covered with a 1.27×10^{-2}-cm (0.005-in.) thick aluminized Mylar sheet that is connected to the plate edges with aluminized Kapton tape. The plate and the radiation shields are connected to the frame with 0.041-cm-diam Dacron tendons. The tendons are spring loaded at the four frame extensions to maintain the correct tension and to accommodate thermally induced dimensional changes. The shields are constructed of 1.27×10^{-2}-cm (0.005-in.) thick Mylar, vapor-deposited with a thin layer of aluminum (about 800 Å) on both sides. A planet shade, sized for the AMTS orbit,[8] is attached to the frame with four fiberglass-epoxy tubes that provide the necessary thermal isolation from the frame. The back of the frame is covered by a multilayer insulation (MLI) blanket to minimize the heat load to the vacuum chamber and to help maintain a uniform frame temperature.

To simulate a typical spacecraft boundary temperature, the outer frame temperature is thermostatically controlled throughout the test to 17°C (290 K) with 34 resistance heaters. The frame is constructed with thick (0.3175-cm) aluminum plates in order to maintain a uniform temperature. The four sides of the frame can be maintained within 1°C of each other during the test. For a low mass flight cooler, the frame may be constructed with a tubular fiberglass-epoxy structure with aluminized Mylar sheets attached. Alternatively, the cold stage plate and radiation shields may be attached to extensions connected to the instrument body, eliminating the need for a separate frame structure. Either way, an actual flight radiator would not require the heaviest part of the thermal engineering model: the aluminum frame.

The planet shade temperature is controlled with six resistance heaters and can be varied to simulate different orbital temperatures. As for the support frame design, the heavy aluminum plates used for the planet shade may be replaced in an actual flight radiator by lightweight aluminized Mylar sheets connected to a tubular frame.

Kapton film heaters are bonded to the back of the cold stage radiator plate. The heater input power can be varied to simulate various instrument heat loads.

Twenty-five type E chromel-constantan thermocouples are located on the cooler engineering model at the approximate locations shown in Fig. 4. Forty gage (0.0076-cm) thermocouples are used to minimize the heat leaks down the wires. Four thermocouples are located on the frame, 3 on the shade, 5 on the cold stage plate, and 13 on the aluminized Mylar shields. Adequate heat sinking and adhesion to the shields is obtained by soft-soldering each junction to disks of ¼-in.-diam copper tape. The copper tape is then placed at the appropriate location on the shields and covered with aluminized Kapton tape. The accuracy of the temperature readings is approximately within ±0.5° C.

The thermocouple channels are monitored once every minute by a Fluke model 2240B data-logger. The data-logger converts analog voltage measurements to temperatures and outputs the resulting values to an HP 1000E minicomputer. The temperatures are continually output to a CRT display and are also recorded on disk. A graphics capability enables

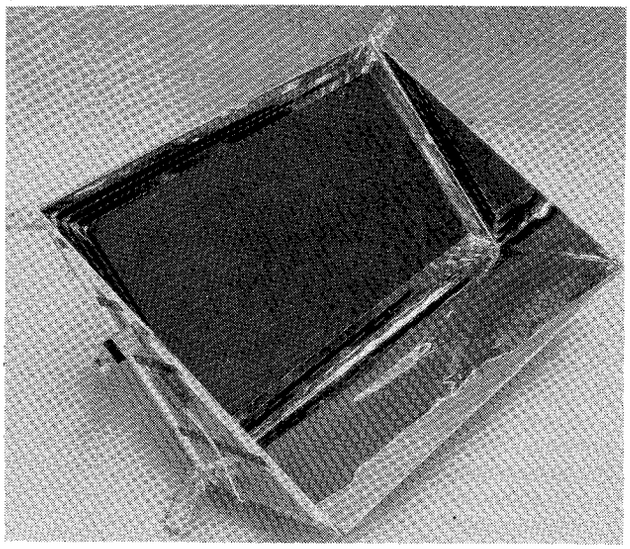

Fig. 3 Advanced passive radiator thermal engineering model.

plotting of test temperatures as a function of time while the test is in progress. The HP 1000E is programmed to control and monitor the heater power for the frame and shade. Two identical HP 6299A dc power supplies (120 V, 0.75 A) drive the frame and shade heater circuits. An HP 6115A precision power supply inputs power to the cold stage radiator plate heaters ($P \pm 0.3$ mW) and outputs the current and voltage values for display on an HP 3450A digital multifunction meter.

The test chamber for this experiment is a 3×3-m liquid nitrogen (LN_2) cooled ion chamber. In the future, a liquid helium (LHe) chamber test, which would better simulate the space environment, is planned. However, an LN_2 test can verify the analytical model and confirm the advanced passive radiator concept. The vacuum pressure in the chamber during the test was 3×10^{-8} Torr. The effective environment temperature is obtained to within ± 0.5°C by averaging two thermocouple measurements of a black aluminum sphere suspended (but conductively isolated) from the top center of the chamber.

Thermal Analysis

Radiator Analysis

The concept test and the detailed numerical model[2] indicated that only four aluminized Mylar radiation shields are required to thermally isolate the cold stage radiator plate from the hot spacecraft (simulated by the aluminum frame in the radiator engineering model). If the cold stage radiator plate is almost thermally isolated from the frame, then the detailed radiation shield node temperatures are not of great interest or importance, and a simple four-node thermal model is adequate. A steady-state energy balance on the cold stage radiator plate, equating the net energy emitted with the energy absorbed from the planet shade, frame, environment (e.g., the vacuum chamber), and the instrument power dissipation gives

$$\mathfrak{F}_{R-E} A_R \sigma (T_R^4 - T_E^4) = \mathfrak{F}_{R-S} A_R \sigma (T_S^4 - T_R^4) + \mathfrak{F}_{R-F} A_R \sigma (T_F^4 - T_R^4) + C_{R-S}(T_S - T_R) + C_{R-F}(T_F - T_R) + P \quad (1)$$

The first two terms on the right represent the radiative heat loads, and the third and fourth terms represent the conductive heat loads from the shade and support frame to the cold stage plate.

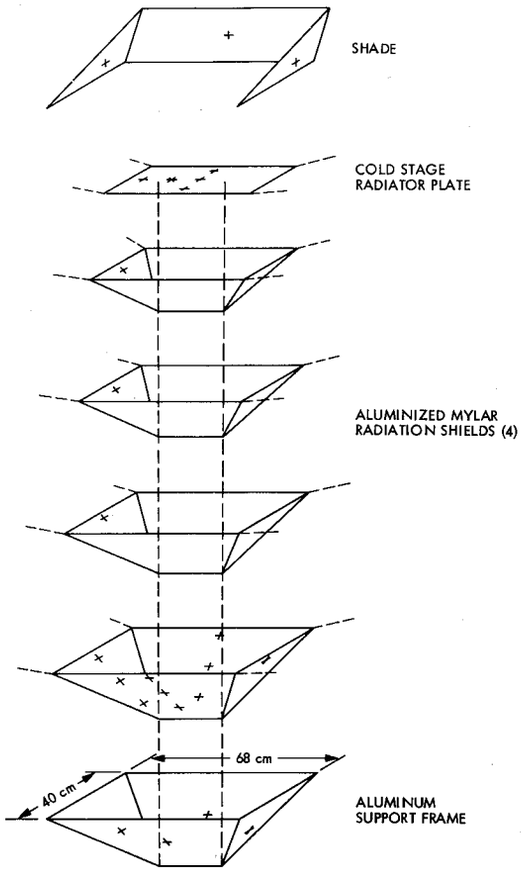

Fig. 4 Exploded view of advanced passive radiator thermal engineering model: thermocouple locations (+), Dacron support tendons (---).

The configuration factor between the radiator plate and specular planet shade is obtained from Monte Carlo[2] techniques as $\mathfrak{F}_{R-S} = 7.3 \times 10^{-3}$. For the plate to the environment, $\mathfrak{F}_{R-E} \simeq \epsilon_R$ (the plate emissivity) $\simeq 0.85$. The conductance from the plate to the frame is made up of contributions from four Dacron support tendons (0.04 cm in diameter) and five chromel-constantan thermocouples (7.6×10^{-3} cm in diameter) with two wires per thermocouple. The lengths of the thermocouple wires and Dacron tendons are about 2.5 cm. The resulting conductance is $C_{R-F} = 9.7 \times 10^{-6}$ W/K. The conductance value between the radiator and shade of $C_{R-S} = 1.8 \times 10^{-5}$ W/K is due to the 7.6×10^{-3}-cm-diam plate heater wires that were routed to the shade (23 cm long).

Equation (1) was solved numerically for the various shade temperatures and power inputs used during the test. In order to determine the effectiveness of the radiative shielding design, the second term on the right-hand side of Eq. (1) was eliminated. The radiator engineering model test results were then compared to this ideal, completely radiatively isolated, analytical model.

Engineering Model Planet Shade Analysis

The inside shade surface was to be coated with vapor-deposited aluminum in order to lower its emittance, but this proved to be too difficult with the available aluminizing chamber facility. The inside shade surface was lined instead with single-sided aluminized Mylar sheets. Temperature measurements from thermocouples mounted on the aluminum shade were then used to calculate the temperature of the lining, based on the analysis in the Appendix. The lining temperature, calculated as $0.84 T_s$ in the Appendix, is substituted for T_s in Eq. (1).

Table 1 Advanced passive radiator test results and comparisons to thermal model predictions

Test run	Radiator power input, W	Environment temperature, K	Planet shade temperature Aluminum, K	Planet shade temperature Lining, K	Radiator temperature Test, K	Radiator temperature Prediction, K	ΔT,[a] %
1	0.0	96.1	160.0	134.0	97.6	96.8	0.8
2	0.05	95.7	160.0	134.0	98.2	97.9	0.3
3	0.088	95.5	160.0	134.0	99.1	98.9	0.2
4	0.20	95.1	160.0	134.0	102.2	101.8	0.4
5	0.0	94.8	201.4	169.0	96.8	96.7	0.1
6	0.0	94.8	224.7	188.0	97.1	97.7	0.6

[a] $\Delta T = |(T_{test} - T_{predict})/T_{predict}|$.

Table 2 Cold stage heat balance (test run 3)

Simulated detector power dissipation, mW	88.0
Planet shade radiation, mW	16.7
Planet shade conduction, mW	0.6
Support frame radiation, mW	10.6
Support frame conduction, mW	1.9
Total cold stage heat rejection, mW	117.8

Results

Six test runs were completed with various power inputs and shade temperatures. For the initial test run, it took about 26 h (including the vacuum chamber cooldown time) for the radiator to achieve steady-state conditions. Steady state was defined here as an average radiator plate temperature change of ≤ 0.1 K in 2 h. The average time to achieve steady state for each subsequent test run was about 8 h.

One anomalous thermocouple reading ranged from 1.7 to 2.2 K above the four other radiator plate thermocouple temperatures throughout the test. The standard deviation of the average of the four remaining plate thermocouples ranged between 0.1 and 0.2 K during the test. The plate was originally designed to be thick enough to minimize any temperature gradients. The location of the anomalous thermocouple, indicated by an asterisk in Fig. 4, combined with the excellent agreement between the four remaining thermocouples, makes the anomalous reading suspect. Because of the difficulty of disassembling and reassembling the radiator in order to look for some physical irregularity, such as inadequate thermocouple attachment and heat sinking to the plate, no further investigation into the cause of the anomalous thermocouple was made. The anomalous thermocouple readings were not included when computing the average radiator plate tem-

Table 1 presents the measured test temperatures for the various cases. The radiator plate temperatures in column 6 are averaged readings of the four plate thermocouples. The average radiator plate temperatures range from 1.5 to 7.1 K above the chamber environment temperatures (measured average black sphere temperatures) listed in column 3. The input power to the radiator ranged from 0 to 200 mW, as indicated in column 2. The 88-mW heat input for the third test run simulates the AMTS heat load for this one-third scale (based on area) engineering model. Columns 4 and 5 contain the measured aluminum shade temperature and the shade lining temperature determined from Eqs. (A1), respectively. The standard deviation of the shade temperature measurements, based on the three shade thermocouples, was less than 0.8°C for each run. Column 7 shows the steady-state cold stage temperature predicted by the analytical model [Eq. (1)] for the ideal radiator. The measured cold stage temperatures are all within 1% of the ideal values, as indicated in the final column.

The temperature predictions for the ideal radiator shown in Table 1 assume complete radiative isolation between the radiator plate and the frame, thus neglecting the second term on the right side of Eq. (1). The actual effect of the second term in Eq. (1), which gives the radiative interaction between the frame and radiator plate, can be determined by substituting the measured radiator temperatures into Eq. (1) and solving for $\mathcal{F}_{R-F}$ (which is equivalent to the effective emittance of the shield assembly, ϵ_{eff}). The angled radiation shield effective emittance, averaged over the six test runs, is thus obtained as $\epsilon_{eff} = 1.5 \times 10^{-4}$. This is over an order of magnitude lower than that achieved by the best existing multilayer insulation blankets that have ever been used in flight.[9] The lowest value achieved by calorimeters,[9] which are ideal since they have few blanket discontinuities, is 10^{-3}.

An error analysis based on experimental standard deviation values of 0.8, 0.11, and 0.5 K for the shade, plate, and environment temperatures, respectively, indicates that the standard deviation of ϵ_{eff} is about 2.2×10^{-4}. There is a 95% level of confidence that the actual value of ϵ_{eff} is less than 4.2×10^{-4}.

The radiator energy balance is summarized for the 88-mW AMTS simulation (test run 3) in Table 2. The support frame radiation and conduction contribute approximately 11% of the total cold stage heat load. The radiative heat leak may be reduced further with improvements in the radiation engineering model, as discussed in the next section.

Discussion

Performance Predictions

For a liquid helium vacuum chamber test with an environment temperature of 30 K and a 160 K shade temperature, the analytical model with $\epsilon_{eff} = 1.5 \times 10^{-4}$ predicts a radiator temperature of 65.3 K for 88-mW power input, and 53.4 K for zero-power input. There were minor fabrication flaws in the engineering model. Some buckling and crinkling of the frame and shade linings occurred, and the radiation shields made contact with each other at several locations. Eliminating the linings by directly aluminizing the shade and frame, and installing the shields more accurately, should enhance the radiator performance and essentially completely radiatively isolate the radiator plate from the frame. Even without improvements, the addition of one more shield may completely radiatively isolate the radiator plate from the frame. In space, with the predicted radiative isolation, the radiator temperature should reach 63 and 51 K for $P = 88$ and 0 mW, respectively.

Radiator Comparisons

Table 3 summarizes size, mass, temperature, and cooling capacity comparisons of the advanced passive radiator with the AMTS radiator[8] and a large, high-capacity state-of-the-art two- and three-stage ground-tested cryogenic radiator test unit (CRTU) developed for geosynchronous Earth orbit.[5,6] Note that the advanced passive radiator designed for the CRTU orbit requires a smaller and colder planet shade, and can thus achieve a lower minimum possible temperature, than that designed for the AMTS orbit.

Table 3 Predicted performance comparisons

Radiator	Radiator temperature, K	Cold stage heat load, W	Projected area, m^2	Radiator mass, [a] kg	Orbit, km
APR	70	5.05[b]	4.6	30	36,000
CRTU, [6] two-stage	70	5.0	8.1	83	36,000
APR	40.5	0.2	2.0	13	36,000
CRTU, three-stage	40.5	0.2	8.1	99	36,000
APR	63	0.26	0.65	5	833
AMTS[8]	63	0.26	5.0	45	833

[a] Projected flight model mass. [b] Includes 50-mW heat pipe parasitic heat leak as assumed for the CRTU.

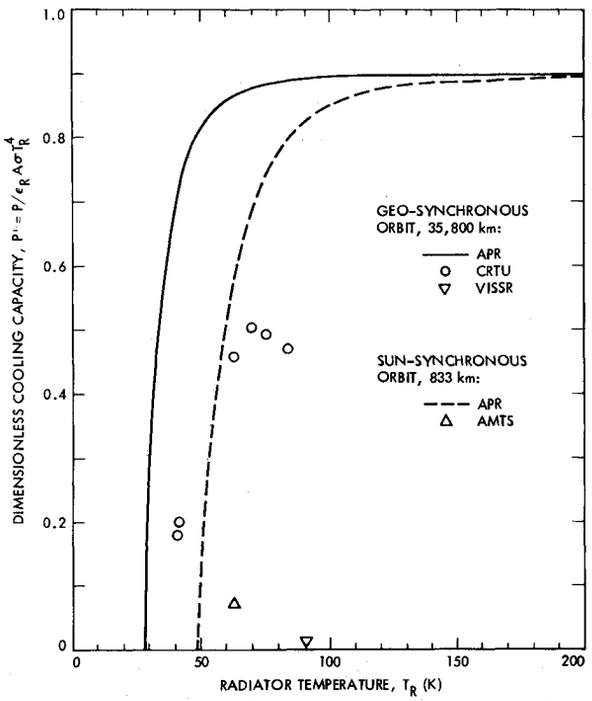

Fig. 5 Advanced passive radiator (APR) performance predictions and comparisons presented in terms of dimensionless cooling capacity as a function of temperature.

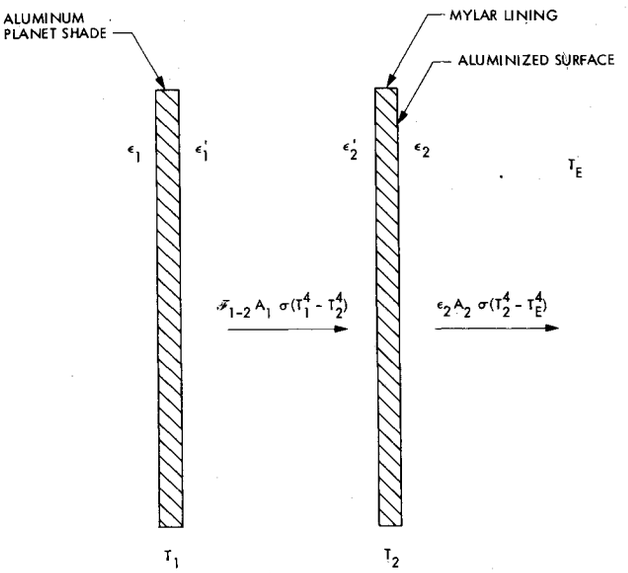

Fig. A1 Planet shade lining energy balance.

Achievement of a temperature of 63 K with 88 mW heat input with the thermal engineering model indicates that a flight model advanced passive radiator can meet the AMTS cooler goals with only 13% of the projected area and 10% of the weight of the proposed AMTS radiative cooler.[8] With appropriate orientation and shading from external heat loads, the advanced passive radiator is predicted to dissipate a 5-W detector heat load at 70 K with 57% of the size and 36% of the weight of the CRTU. The potential 3.5-m^2 and 53-kg reductions in size and mass, with respect to the CRTU, should make radiative cooling more feasible for these cooling requirements. In practice, achievement of 40.5 K with an actual Earth-orbiting flight radiator may not be feasible, but the 2-m^2 advanced passive radiator would be easier to shield from the hot spacecraft, Earth, and sun than the 8.1-m^2 three-stage CRTU.

Previously reported comparisons indicate[2] that the advanced passive radiator has approximately 500% more cooling capacity, for the same temperature and mass, than certain conventional radiative coolers flown in the past (VISSR, 1974).[3] A convenient method of presenting these radiator comparisons is to plot dimensionless cooling capacity as a function of cold stage temperature for each cooler, as shown in Fig. 5. The radiator cooling capacity has been normalized with respect to the heat rejected by an ideal radiator plate (i.e., a plate with no internal or external parasitic heat inputs), giving $P' = P/\epsilon_R A\sigma T_R^4$. The design goal of any radiative cooler is to have a dimensionless cooling capacity approaching $P' = 1$. Advanced passive radiator performance predictions are shown for both a 35,800-km geosynchronous orbit and an 830-km sun-synchronous orbit. The CRTU and VISSR data[5,3] must be compared to the advanced passive radiator geosynchronous orbit curve, while the AMTS cooler performance prediction is compared to the sun-synchronous advanced cooler curve. The higher cooling capacity of the advanced radiator with respect to the other coolers is clearly indicated. At the lower temperatures, the advanced passive radiator temperature is limited by the external heat inputs from the planet shade. At higher operating temperatures, the cooling capacity is limited by the radiator projected area occupied by the angled shield openings.

A final qualitative comparison deals with contamination. The large areas of multilayer insulation (MLI) used on many conventional radiators, such as the CRTU, are prime sources, as well as traps, for water vapor. In space, the water vapor evaporates from the MLI and condenses onto and contaminates nearby cold surfaces, such as the optics, detectors, and the cold radiator stage. By completely eliminating MLI, the advanced passive radiator should have fewer contamination problems than conventional radiative coolers. One effect of contamination may be a rise in the emissivity, or a decrease in the specularity of the radiation shield surfaces. Previous sensitivity studies[2] indicated that even a 100% increase in shield emissivity or a 20% decrease in specularity results in less than a 10% increase in the radiator temperature.

Figure 5 may be used to predict the approximate advanced passive radiator size for various applications. Refer to the high or low Earth orbit curves, as is appropriate for the specific application. The advanced passive radiator curves have not been optimized with respect to the ideal number of

shields. For a given overall size, the size of the radiator plate can be increased by reducing the number of shields. Reducing the number of shields increases the parasitic heat loads. Clearly, these factors operate in opposite directions, and some optimum design point will prevail for any particular application.

Intelligent spacecraft integration is necessary for any passive radiator. This includes some control of cooler location, spacecraft configuration and orientation, and the addition of shading to reduce external heat inputs. The greatly reduced size of the advanced passive radiator relative to other radiative coolers makes the systems integration task easier and should extend the practical range of applicability of passive radiators from the presently accepted limit of 70 K (Ref. 1) to below 60 K.

Conclusions

Thermal vacuum chamber experiments indicate that the advanced passive radiator has the ability to greatly reduce the internal parasitic conductive and radiative heat leaks to the cold radiator stage and thus offers the potential for considerable size and weight reductions for future long-lifetime spaceborne passive radiative instrument coolers. Cold stage temperatures measured in the thermal engineering model test were all within 1% of analytical model predictions and range between 1.5 and 7.1 K above the vacuum chamber environment temperature, as indicated in Table 1.

The thermal isolation capability of the angled radiation shield assembly is demonstrated by its effective emittance, approximated from the test results as 1.5×10^{-4}. This value is an order of magnitude lower than that achieved by the best existing multilayer insulation blankets ever used in flight. Based on these experiments and an analytical thermal model, performance predictions presented in Table 3 and Fig. 6 indicate that the advanced passive radiator would be between 10 and 57% of the size and mass of the best state-of-the-art radiative coolers. With its reduced size and mass and increased cooling capacity, the advanced passive radiator can meet many of the new spaceborne instrument cooling requirements and should achieve practical operating temperatures below 60 K.

Appendix: Planet Shade Lining Analysis

An energy balance on the single side aluminized Mylar lining, as shown in Fig. A1, gives

$$\epsilon_2 A_2\sigma(T_2^4-T_E^4)=\mathfrak{F}_{2-1}A_2\sigma(T_1^4-T_2^4) \qquad \text{(A1a)}$$

or

$$\frac{T_2}{T_1}=\left(\frac{\mathfrak{F}_{2-1}+\epsilon_2(T_E/T_1)^4}{\epsilon_2+\mathfrak{F}_{2-1}}\right)^{1/4} \qquad \text{(A1b)}$$

Here we assume the shade and lining behave as parallel plates, giving

$$\mathfrak{F}_{2-1}=1\frac{1-\epsilon_1'}{\epsilon_1'}+\frac{1}{F_{1-2}}+\frac{1-\epsilon_2'}{\epsilon_2'} \qquad \text{(A2)}$$

where T_1 is the aluminum shade temperature; T_2 the aluminized Mylar lining temperature; ϵ_1' the emissivity of aluminum shade surface facing Mylar (see Fig. A1); ϵ_2' the emissivity of Mylar lining surface facing aluminum; ϵ_2 the emissivity of aluminized Mylar lining surface facing radiator plate; and F_{1-2} the radiation shape factor from surface 1 to 2 (equals 1 here).

Conduction between the shade and lining has been neglected in Eqs. (A1), since it is assumed that they touch only at the very edges and the Mylar is just 0.0064-cm (0.025-in.) thick, with a thin (less than 800-Å) layer of aluminum on one side. The aluminum and lining emittances, measured at room temperature, are $\epsilon_1'=0.05\pm0.03$, $\epsilon_2'=0.74\pm0.15$, and $\epsilon_2=0.02\pm0.02$. Substituting these values into Eqs. (A1) and (A2), with $T_E=95$ K and $T_1=160$ K, gives $\mathfrak{F}_{2-1}=0.049$ and $T_2/T_1=0.93\pm0.09$. The resulting accuracy of T_2/T_1 is not very sensitive to uncertainties in ϵ_1', ϵ_2', and ϵ_2. For example, if $\epsilon_1'=0.04$ and $\epsilon_2=0.05$, with $\epsilon_2'=0.6$, then $T_2/T_1=0.84$. Assuming too high a shade temperature will underestimate the actual internal parasitic heat leak to the cold stage plate, so a conservatively low value of $T_2/T_1=0.84$ is assumed. For the future LHe chamber test, the inside aluminum shade surface will be aluminized directly. Thus the desired temperature will be measured, thereby avoiding the present ambiguity.

Acknowledgments

The research described in this paper was carried out at the Jet Propulsion Laboratory, California Institute of Technology, under NASA Contract NAS7-100. The author wishes to thank Dr. A. A. Kudirka, S. W. Petrick, and Dr. R. P. Salazar for their assistance and many useful suggestions; Dr. D. Elleman for his support; and L. Bennett, D. Lewis, W. Walker, E. Gillespie, and especially T. Patrick for their instrumentation, fabrication, and technical assistance.

References

[1] Sherman, A., "History, Status and Future Applications of Spaceborne Cryogenic Systems," *Advances in Cryogenic Engineering*, Vol. 27, 1981, p. 1007.

[2] Bard, S., Stein, J., and Petrick, S. W., "Advanced Radiative Cooler With Angled Shields," *Progress in Astronautics and Aeronautics: Spacecraft Radiative Transfer and Temperature Control*, Vol. 83, AIAA, New York, 1982, pp. 249-258.

[3] Donahoe, M., Sherman, A., and Hickman, D., "Radiant Coolers-Theory, Flight Histories, Design Comparisons, and Future Applications," AIAA Paper 75-184, Pasadena, Calif., Jan. 1975.

[4] Hulett, R. H. and Zierman, C. A., "Staged Radiator Design for Low Temperature Spacecraft Applications," AIAA Paper 70-854, Los Angeles, Calif., June 29-July 1, 1970.

[5] Wright, J. P., Wilson, D. E., and Lehtinen, A. M., "Cryogenic Radiator Test Unit," Flight Dynamics Laboratory, Wright-Patterson AFB, Ohio, AFWAL-TR-80-3124, Dec. 1980.

[6] Wright, J. P., "Development of 5-Watt 70°K Passive Radiator," AIAA Paper 80-1512, Snowmass, Colo., July 14-16, 1980.

[7] Merriam, R. and Gabron, F., "Spaceborne Passive Radiators for Detector Cooling," ASME Paper 71-AV-30, 1971.

[8] Salazar, R. P. and Evans, N., "A Study of a 63 K Radiative Cooler for the Advanced Moisture and Temperature Sounder," AIAA Paper 81-1101, June 1981.

[9] Stimpson, L. D. and Jaworski, W., "Effects of Overlaps, Stitches, and Patches on Multilayer Insulation," *Progress in Astronautics and Aeronautics: Thermal Control and Radiation*, Vol. 31, MIT Press, Cambridge, Mass., 1973, pp. 247-266.